J. Fluid Mech. (2011), *vol.* 685, *pp.* 440–460.
doi:10.1017/jfm.2011.328

Wall shear stress in accelerating turbulent pipe flow

S. He[1]†, C. Ariyaratne[2] and A. E. Vardy[3]

[1] Department of Mechanical Engineering, University of Sheffield, Sheffield S1 3JD, UK
[2] Thermo-Fluid Mechanics Research Centre, University of Sussex, Brighton BN1 9QT, UK
[3] Division of Civil Engineering, University of Dundee, Dundee DD1 4HN, Scotland, UK

(Received 11 June 2010; revised 6 May 2011; accepted 28 July 2011;
first published online 21 September 2011)

An experimental study of wall shear stress in an accelerating flow of water in a pipe ramping between two steady turbulent flows has been undertaken in a large-scale experimental facility. Ensemble averaged mean and r.m.s. of the turbulent fluctuations of wall shear stresses have been derived from hot-film measurements from many repeated runs. The initial Reynolds number and the acceleration rate were varied systematically to give values of a non-dimensional acceleration parameter k ranging from 0.16 to 14. The wall shear stress has been shown to follow a three-stage development. Stage 1 is associated with a period of minimal turbulence response; the measured turbulent wall shear stress remains largely unchanged except for a very slow increase which is readily associated with the stretching of existing turbulent eddies as a result of flow acceleration. In this condition of nearly 'frozen' turbulence, the unsteady wall shear stress is driven primarily by flow inertia, initially increasing rapidly and overshooting the pseudo-steady value, but then increasing more slowly and eventually falling below the pseudo-steady value. This variation is predicted by an analytical expression derived from a laminar flow formulation. The start of Stage 2 is marked by the generation of new turbulence causing both the mean and turbulent wall shear stress to increase rapidly, although there is a clear offset between the responses of these two quantities. The turbulent wall shear, reflecting local turbulent activities near the wall, responds first and the mean wall shear, reflecting conditions across the entire flow field, responds somewhat later. In Stage 3, the wall shear stress exhibits a quasi-steady variation. The duration of the initial period of nearly frozen turbulence response close to the wall increases with decreasing initial Reynolds number and with increasing acceleration. The latter is in contrast to the response of turbulence in the core of the flow, which previous measurements have shown to be independent of the rate of acceleration.

Key words: boundary layer, pipe flow, unsteady, wall shear stress

1. Introduction

Unsteady turbulent flows in pipes and channels include periodic and non-periodic flows. Both cases have been studied experimentally as well as theoretically, but greater

† Email address for correspondence: s.he@sheffield.ac.uk

attention has been paid to periodic flows. This is justified in the sense that many practical applications involve pulsations. However, non-periodic flows with uniform acceleration/deceleration have advantages for unravelling the non-equilibrium behaviour of turbulence dynamics in unsteady flows. This paper focuses on near-uniform accelerating flows and, in particular, on the response of the wall shear stress to acceleration.

Detailed studies of *pulsating* flows in pipes have been described by, for example, Gerrard (1971) and Ronneberger & Aherens (1977), followed by Tu & Ramaprian (1983), Shemer, Wygnanski & Kit (1985) and, more recently, by Scotti & Piomelli (2001) and He & Jackson (2009). Tardu and coworkers conducted a series of studies of flows in channels (Tardu & Binder 1993; Tardu, Binder & Blackwelder 1994; Tardu & Da Costa 2005), Brereton, Reynolds & Jayaraman (1990) and Brereton & Reynolds (1991) studied pulsating flows of a developing boundary layer.

Studies of *wall shear stress* in pulsating flows have been undertaken by a number of researchers, including Mao & Hanratty (1986, 1992) for pipe flows and Tardu & Binder (1993) and Tardu *et al.* (1994) for channel flows. Mao and Hanratty used an electrochemical technique to measure wall shear stresses in a 194 mm diameter pipe for a range of pulsating frequencies ($\omega^+ = 0.0075$–0.21, where $\omega^+ = \omega\nu/u_\tau^2$). Tardu and coworkers used flush mounted hot-film anemometry to measure wall shear stresses in flows in a channel of cross section of 100 mm $\times$ 1000 mm. These papers reported outcomes for high-frequency (up to $\omega^+ = 0.24$) and low-frequency ($\omega^+ < 0.03$) ranges, respectively. It has been established that, for pulsating flows with a non-zero mean flow, the long time averaged mean and root mean square (r.m.s.) of turbulent fluctuations of the wall shear stress (referred to hereafter as the turbulent wall shear stress) are unaffected by pulsation of the flow, but that the phase-averaged mean wall shear stress lags behind the centre-line velocity. This phase lag varies from almost zero at very low frequencies (approaching quasi-steady flow) to about 45° for a Stokes flow at $\omega^+ = 0.02$–0.045, but then decreases with further increases of frequency. In the case of slow pulsations, the amplitude of the phase averaged wall shear stress is significantly greater than that predicted using Stokes' theory. However, it decreases with increasing frequency and, at sufficiently high frequencies, it is smaller than that in Stokes flow. The phase-averaged wall shear stress is found to be well represented by the fundamental harmonic component, but the phase-averaged turbulent wall shear stress intensity is not. It exhibits a more nonlinear response, although the fundamental mode still contains more energy than higher modes. Tardu & Binder (1993) showed that the amplitude of the modulation of the turbulent wall shear relative to quasi-steady values reduces from unity to around 0.1 as ω^+ increases from zero (quasi-steady flow) to around 0.02. With further increases in frequency, however, the amplitude increases again and reaches around 0.6. The time lag ($t^+ = tU_\tau^2/\nu$) between the phase-averaged mean wall shear stress and the corresponding turbulent shear stress intensity is found to be constant (around 130) for all medium and low frequencies, but it increases when ω^+ exceeds $\sim$0.025, which is of the order of the turbulent burst frequency. Tardu and Binder considered the above results to be an indication that interactions between the imposed flow pulsation and turbulence cause an enhancement in turbulence.

Non-periodic unsteady flows in which a turbulent flow increases or decreases monotonically have been studied experimentally by Maruyama, Kuribayashi & Mizushima (1976), Greenblatt & Moss (1999, 2004) and He & Jackson (2000), and numerically, using direct numerical simulation (DNS), by Chung (2005). In addition, Piomelli, Balaras & Pascarelli (2000) studied spatially accelerating flow numerically. Many of the experimental observations can be related to turbulence responses,

including turbulence production near the wall, turbulence energy redistribution among the components and radial propagation into the core of the flow. In particular, the finite time scales of these activities cause 'delays' that characterize the response of turbulence. As a result, the response at any radial location exhibits a three-stage development, namely a delay (during which the turbulence remains largely frozen), a rapid response and a 'developed' stage. In comparison with quasi-steady flow, the turbulence intensity tends to be reduced in an accelerating flow and increased in a decelerating flow, mainly due to delayed responses of turbulence. For a rapidly accelerating flow, Greenblatt & Moss (2004) found that turbulence production could first occur at a location well beyond the buffer layer (say $y^+ = 300$) and that the new turbulence propagates towards the wall as well as into the core of the flow. They regarded this as a consequence of a strongly distorted velocity profile.

Measurements of *wall shear stresses* in non-periodic unsteady flows are very sparse. Shuy (1996) presented an experimental study of wall shear stress in a pipe. He found that the wall shear stress was smaller than the quasi-steady value in accelerating flows and greater than the quasi-steady value in decelerating flows. This 'contradicted' the predictions of widely used unsteady friction models, e.g. Vardy & Brown (2003), and led to discussions contributed by several authors, including Proudovsky (1997) who revealed several studies carried out in former USSR, which were largely documented in Russian but were also summarized in English at international conferences, e.g. Ainola *et al.* (1983) and Proudovsky & Oreshkin (1985). These studies showed that the wall shear stress in an accelerating flow is initially greater than the corresponding quasi-steady values, but that it subsequently becomes smaller. This behaviour is supported by experimental data presented by He & Jackson (2001). Whereas the above qualitative picture of unsteady wall shear stress variation is now widely accepted, quantitative analysis is still at a preliminary stage and there is a lack of systematically conducted experiments to assist in its development.

The present authors reported a numerical study of wall shear stresses in accelerating pipe flows using a Reynolds averaged Navier–Stokes (RANS) modelling approach incorporating a low Reynolds number turbulence model (He, Ariyaratne & Vardy 2008). Predictions for systematically varied flow conditions (including acceleration, Reynolds number, fluid and dimensions) were consistent with the experimental observations described above. In each case, the wall shear stress first overshoots and then undershoots the quasi-steady value before approaching an asymptotic state quite close to quasi-steady conditions. This characteristic behaviour was attributed to two mechanisms, namely (i) inertia and (ii) delays in the response of turbulence to changes in the mean flow. The numerical results, which were validated by comparison with available measurements in the core of the flow, led to increased understanding of turbulence dynamics in unsteady flows. The influence of varying flow conditions on wall shear response was predicted although the primary emphasis was on qualitative rather than quantitative trends (acknowledging potential limitations of turbulence models).

The objective of the present paper is to present results of a detailed experimental study of wall shear stress using flush-mounted hot-film sensors in an accelerating flow in a large-scale flow loop. Ensemble averaging was performed based on measurements from many repeated runs. This has yielded definitive measurements of mean wall shear stresses and has established experimentally the characteristics of wall shear stress responses for a range of flow conditions. It has also provided measurements of turbulent wall shear stress that extend the body of data on turbulence in non-periodic flows, currently available only in the core of the flow, thereby helping to

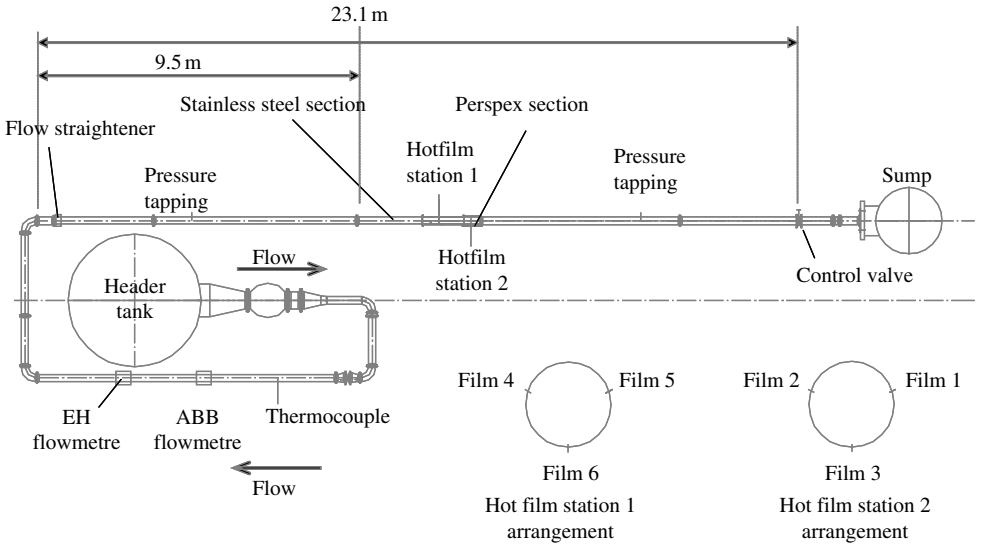

FIGURE 1. Plan view of the experimental facility.

develop a fuller understanding of the flow behaviour. The behaviours of the mean wall shear stress and the turbulent wall shear stress are characterized and key features are correlated using a normalized acceleration parameter.

2. Experimental arrangement

The experiments were undertaken in a large-scale flow loop (figure 1) in which water was supplied from a 28 m high, 1 m diameter constant-head tank. Detailed flow control was achieved using a computer-operated, pneumatically driven globe valve at the end of a long test section. Water discharged from the pipe was collected in a large sump, from which it was pumped back to the water tower. The test section was within a length of straight pipe, 23 m long and 206 mm in diameter. Most of the pipe was formed from flush-connected, galvanized-steel tubes, but the main measurement region was a 300 mm long Perspex tube immediately downstream of a 3.25 m long stainless steel pipe. These sections had the same nominal diameter as the galvanized steel pipe. The Perspex section was manufactured by an external specialist company to ensure that the internal diameter (i.d.) of the two sections were closely matched. A 150 mm long honeycomb flow straightener made of 12 mm i.d. stainless steel tubes was located at the beginning of the straight pipe section to eliminate any large-scale swirl caused by bends further upstream. The main measurement section was placed in the middle of the long section because some of the experiments within the series (not reported here) involved flow in the reversed direction.

Each accelerating flow case is defined by the initial and final Reynolds numbers (Re_0, Re_1) and by the duration of the ramp (T). During each experiment, the flow was initially held steady for 60 s at the prescribed initial Reynolds number Re_0. It was then ramped up at an approximately constant rate in an interval T by gradually opening the control valve in a pre-determined manner and was then held constant at a Reynolds number Re_1 for a further 30 s. This procedure was repeated many times to enable ensemble averaging to be performed. Experiments were conducted for several values of Re_0, Re_1 and T, corresponding to values of a non-dimensional acceleration

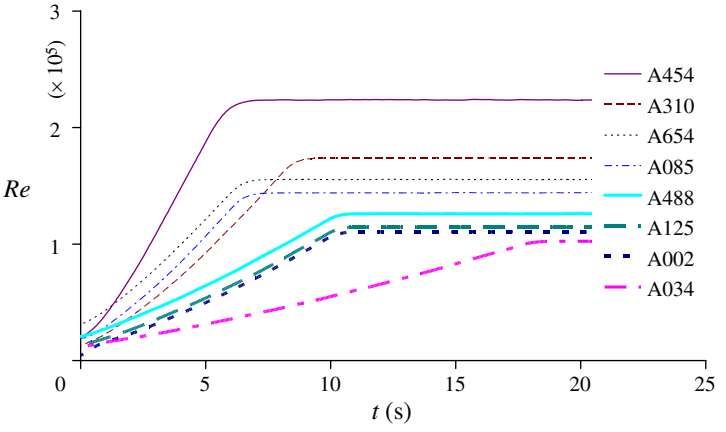

FIGURE 2. (Colour online available at journals.cambridge.org/flm) Flow histories of the various test cases.

Case	Number of repeats	Re_0	Re_1	T (s)	δ	k
A310	117	13 200	160 000	7.9	0.094	1.563
A125	133	11 750	105 000	9.6	0.067	1.093
A002	24	4 500	100 000	9.6	0.973	14.083
A034	39	9 800	97 500	17.3	0.059	0.947
A488	161	20 700	120 000	9.9	0.015	0.260
A085	35	19 300	122 500	5.6	0.033	0.583
A454	33	20 700	210 000	5.6	0.050	0.878
A654	30	31 350	145 000	6.0	0.009	0.162

TABLE 1. Summary of experimental conditions. $\delta = (\nu/U_{\tau 0}^2)(1/U_0)/(\mathrm{d}U/\mathrm{d}t)$, non-dimensional parameter for accelerating flow based on turbulence production time scale (He & Jackson 2000). $k = -(\nu/\rho U_0^3)(\mathrm{d}p/\mathrm{d}x) \approx (\nu/U_0^3)(\mathrm{d}U/\mathrm{d}t)$, non-dimensional parameter for spatially accelerating flow.

parameter $k(k \equiv -(\nu/\rho U_0^3)(\mathrm{d}p/\mathrm{d}x) \approx (\nu/U_0^3)(\mathrm{d}U/\mathrm{d}t))$, ranging from 0.16 to 14. Here, U_0 is the bulk velocity at the start of the acceleration and $\mathrm{d}U/\mathrm{d}t$ is the nominal or mean acceleration of the near-linear accelerating flow. In addition, steady-flow experiments were undertaken for the whole of the flow range covered in the unsteady flows. These data were processed using conventional averaging to provide quasi-steady data for comparison with the accelerating flow cases. A summary of the experimental conditions is given in table 1. Owing to practical constraints, the flow acceleration was not exactly constant. Representative actual flow histories are shown in figure 2.

2.1. *Instrumentation*

The flow loop had two electromagnetic flowmeters, an ABB model 50SM1000 and an Endress–Hauser model Promag 50W. The former was configured to provide instantaneous flow readings. It responded rapidly to flow changes, but its signal tended to be noisy. The latter was configured to measure low-frequency changes and a low-noise signal was assured using filtering and integration techniques. Three differential pressure transducers were used simultaneously to measure the pressure drop along the test section (figure 1). The transducers had different measuring ranges, which were set

to 7.5 mbar, 60 mbar and 600 mbar. This enabled pressure gradients corresponding to a large range of flow rates and accelerations to be measured reliably. The transducers were connected to tappings at locations of 21 and 90 diameters downstream of the honeycomb straightener, which is expected to provide a true representation of the mean pressure drop in spatially developed flows. For example, the hydrodynamic entry length is $\sim 20D$ at Reynolds number 50 000 estimated using the empirical expression of $L - h/D = 1.359Re_D^{1/4}$ (Kasar, Shah & Aung 1987), beyond which the change on wall friction is expected to be small (typically less than 2 %). Although differential pressures were recorded for both steady and unsteady flows, only the steady flow data were used for validating flow measurements. Theoretically, frictional loss can be deduced for unsteady flows by subtracting inertial pressure gradients from measured overall gradients, but this method involves large uncertainties and so it has not been used in the present study.

Wall shear stresses were measured using fast response hot-film anemometry comprising glue-on sensors and a multi-channel constant temperature anemometer (CTA) system all supplied by Dantec Dynamics. The sensors are 0.1 mm in diameter and 0.9 mm long and hence have small inertia. The response rate is estimated to be up to 0.5–1 kHz (depending on flow rate) by the manufacturer. This is typical of liquid flow applications due to the thermal boundary layer around the probe. The hot-film sensors operated in a constant-temperature mode with 45 °C over-heating. This relatively high value was chosen to increase the sensitivity of the measurements. In general, the response of the hot-film sensor used to measure wall shear stress can be an issue of concern due to the attenuation of turbulent fluctuations resulting from conduction through the substrate. Numerous studies have been carried out on this topic over the years, examples of which include an experimental investigation of Ruedi *et al.* (2004), a series of studies by Chew, Khoo and colleagues (e.g. Chew *et al.* 1998), and a numerical study by Tardu & Pham (2005). The problem is pronounced when the ratio of the conductivities of the fluid and substrate is large. As such it is less of a problem with water applications. As shown later, the wall shear stress intensity (i.e. the ratio of the r.m.s. wall shear stress over the mean wall shear stress, τ_w'/τ_w) obtained for steady flows in the present study was ~ 0.4, as would be expected for such flows, thereby confirming satisfactory performance of the sensors used in this application. The sensors were mounted on Perspex plugs shaped to match the curvature of the pipe internal surface. It was ensured that unevenness between the inner surfaces of the pipe and the plug was typically less than 0.1 mm (although, as discussed below, film 3 might have failed to achieve this). Three sensors were installed in each of two axial locations, respectively 11 m and 12 m from the upstream end of the test section. Location 1 was within the stainless steel pipe and location 2 was within the Perspex pipe (figure 1). The three sensors at each station were distributed uniformly (circumferentially) with one at the bottom of the pipe. This avoided placing sensors at the top of the pipe where air bubbles could have led to false readings and to damage from over-heating.

The hot-film sensors were calibrated *in situ* three times a day for a range of steady flows. Each time, the flow was varied, typically, from $Re = 5000$ to 200 000 in around 25 steps, with each step lasting for over 60 s to ensure that the flow reached a steady state. Data were collected throughout the entire period although only those in the last 20 s of each step were used for calibration. Each calibration exercise lasted ~ 30 min. Two sets of wall shear stress measurements (τ_w) were available for use in calibration: (i) τ_w directly obtained from pressure gradient measured from the differential pressure transducers and (ii) τ_w derived from flow measurements in

conjunction with the Haaland correlation. Wall shear stresses obtained by these two methods were found to overlap each other within experimental uncertainty. Although the differential pressure is a more direct measurement of wall shear, careful switching between the three transducers was needed to cover the whole range of flow rate, and hence flow measurements were used for calibration for the data presented in this paper. It was found that the shear stress–voltage calibration curves, one for each sensor, followed the 'standard' relationship $E^2 = A + B\tau_w^n$ quite well, where E is the voltage of the sensors, A and B are calibration constants and $n = 1/3$. However, an alternative expression in the form of $\log(\tau_w) = A' + B'E$, where A' and B' are calibration constants, was found to correlate the data slightly better (i.e. with a smaller deviation) and was therefore used. For very low flow rates, larger scatter was observed and neither of the above expressions was able to correlate the data, so polynomial fitting was used. During the whole period of experiments, four sensors behaved very consistently with very little drift, therefore one calibration for each sensor was used for the entire period. The fifth sensor needed a calibration for each day whereas the last one failed at the beginning of the test programme.

The data acquisition and flow control were computer-based using a 14-bit, multi-channel, analogue–digital converter interface board. In addition to flow rate, differential pressure and hot-film input signals, measurements included the absolute pressure, water temperature and the flow control signal. Data were sampled at a rate of 1 kHz for each channel.

2.2. *Accuracy*

The main sources of potential uncertainty in the experimental measurements are (i) calibration and drifting of the hot-film anemometer, (ii) repeatability of flow control, (iii) disturbance of flow due to misalignment of the hot-film sensors with the wall and (iv) the number of repeat runs available for ensemble averaging.

Calibration errors were mainly associated with the flow measurement. The precision electromagnetic flow meter used had a small uncertainty of $\pm 0.6\,\%$ in the range of flow encountered in this study. Uncertainties caused by drifting were kept small ($<\pm 1\,\%$) by frequently checking and updating the calibration (three times daily). The repeatability of flow control for the multiple runs used for ensemble averaging was controlled to within $\pm 2.5\,\%$ by rejecting occasional bad runs. In case A002, however, the starting Reynolds number was very low (4 500) and the repeatability criterion had to be relaxed to $\pm 13\,\%$ to achieve an adequate number of repeat runs. Misalignment of the hot-film sensors is believed not to be an issue because the readings of the different sensors (except for film 3) are consistent and there are no systematic variations between them. Uncertainty due to the limited number of repeat runs has been reduced by using a 'window-averaging' approach described later. Such uncertainties can be assessed from fluctuations in the statistics (e.g. mean and turbulent wall shear stress) which are easily identified and estimated as shown below.

At low flow rates, another potential source of error in the sensor measurements is locally induced buoyancy due to the heating of the hot-film sensors, resulting in scatter of the calibration data as high as $\pm 10\,\%$ when $Re < 18\,000$. Likewise, in very rapid accelerations, errors might arise from the gradual deviation from the calibration of the hot-film established under steady flow. However a computational fluid dynamics (CFD) analysis (reported elsewhere Ariyaratne *et al.* 2010) has shown that this effect is significant for only a fraction of a second after the start of each flow excursion.

As with many experiments, it is not possible to give a definitive measure of the residual error remaining even after taking the above steps to minimize errors. However,

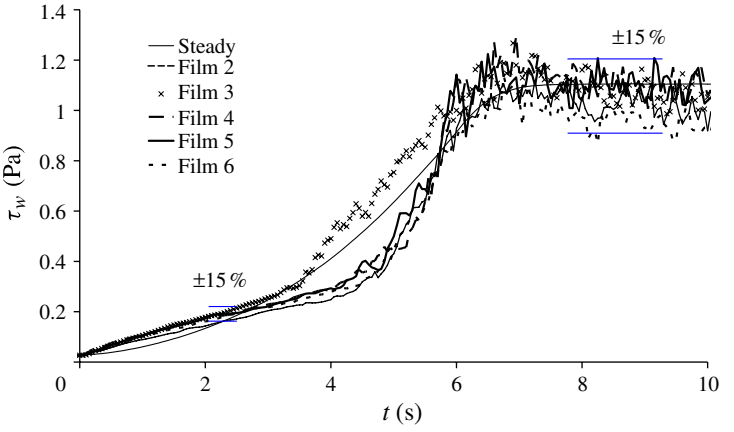

FIGURE 3. (Colour online) Comparison of measurements by the various hot-film sensors in a typical accelerating flow (A085).

the use of multiple hot-film sensors provides one measure of the uncertainties. Figure 3 compares the wall shear stresses measured by the five hot-film sensors in a typical acceleration experiment. Four of the sensors agree reasonably well, but film 3 differs markedly. It is believed that this was caused by a local flow disturbance, either by obstruction of a wire used for bubble generation for particle image velocimetry (PIV) measurements just upstream of film 3, or by misalignment of the sensor, or both. It is noted that the differences between the measurements of film 3 and those of other films occur only during the transition; there are no significant differences in the values before and after the transition (figure 3). To some extent, this demonstrates the robustness of the method adopted here for wall shear stress measurement using flush mount sensors. Overall, random fluctuations of the mean wall shear stress are within $\pm 15\,\%$, which is indicated at two locations in the figure. This is typical of all tests. The fluctuations of the r.m.s. turbulent wall shear stress curves are more pronounced and, for low flow rates, the uncertainty band is nearly doubled.

Ideally a very long test section, say, $150D$ or more, would be preferred to ensure a fully developed flow is achieved and that turbulent quantities are stationary. However, owing to practical limitations, the test section in the present study is $\sim 50D$. This is judged to be sufficient for the purpose of the present study because the variation of the most relevant flow quantities is rather moderate after $50D$ and the wall shear is among the least sensitive variables. As discussed earlier, the hydrodynamic entrance length based on the condition that the change of wall friction is less than $2\,\%$ is $\sim 20D$ for $Re = 50\,000$ (Kasar *et al.* 1987). In the present study, there are no systematic differences between measurements of films at the two stations 1 m apart, thus confirming that the flow is spatially developed at the measurement stations as far as the wall shear is concerned. Further confidence in the reliability of the data is provided by the relatively small scatter in the correlations of the data presented below. In addition, a special focus of the present work is on differences between unsteady and quasi-steady behaviour. These differences are less sensitive to experimental uncertainties than are absolute values.

2.3. *Ensemble average*

For each unsteady flow case, many repeated runs were carried out and the results were used for ensemble averaging. The measured raw voltage signals from the CTA for any hot-film in a run were first converted to wall shear stress using the film-specific calibration curve. These variations of instantaneous wall shear stresses of the various repeated runs were then ensemble-averaged to produce mean and r.m.s. turbulent fluctuations of wall shear stresses. This process was repeated for each film. Consistent results have been obtained from the measurements of the various films as discussed above in relation to figure 3. Unless otherwise stated, film 5 is the source of measurements presented below. Mean values of the measurements from the various films are not presented because this would smooth out sharp variations that are important features of the true flow behaviour.

The window-averaging approach introduced by He & Jackson (2000) was used to further reduce the scatter. This enables the ensemble averaged mean and r.m.s. turbulent fluctuations of any quantity φ to be written as

$$\bar{\varphi}_k = \frac{1}{NM}\sum_{i=1}^{N}\sum_{j=1}^{M}\varphi_{i,j+(k-1)M}, \quad k = 1, 2, 3, \ldots, L \tag{2.1}$$

$$\varphi'_k = \left[\frac{1}{NM}\sum_{i=1}^{N}\sum_{j=1}^{M}(\varphi_{i,j+(k-1)M} - \bar{\varphi})^2\right]^{1/2}, \quad k = 1, 2, 3, \ldots, L \tag{2.2}$$

where L is the number of windows into which a run is divided, M is the number of samples in each window, N is the number of repeats of the flow case and $\varphi_{i,j+(k-1)M}$ is the $[j + (k-1)M]$th sample of the instantaneous quantity for the ith run. In this study, N ranged from 30 to 190. Here M was chosen to be 50 to maximize the data points used for the averaging whilst also ensuring negligible variation of the mean values in each window. It was checked that the mean and r.m.s values were not sensitive to a doubling of the window size. In the paper, τ_w and τ'_w are used to denote the ensemble averaged mean and r.m.s. turbulent wall shear stresses respectively, noting that the overbar for the mean quantity is omitted for simplicity.

3. Results and discussion

3.1. *Responses of ensemble averaged mean and turbulent wall shear stresses: the general picture*

Figure 4 shows evolutions of wall shear stresses (τ_w) in two groups of tests. In one group, the acceleration is nominally the same in each test and the measurements highlight the influence of the initial Reynolds number. In the other, the initial Reynolds numbers are nominally the same and the measurements highlight the influence of acceleration. Corresponding values of measured wall shear stresses in steady flows provide quasi-steady flow curves for comparison with the unsteady flow values. The results are presented in two forms, with axes of time and Reynolds number, respectively.

In all cases, the wall shear stress in the unsteady flow deviates significantly from quasi-steady behaviour. Its development can conveniently be considered in three stages. Consider, for example, the measurements shown for case A310 in figure 4(*b*). Stage 1 extends up to a Reynolds number of ~125 000. Stage 2 is much shorter, namely from ~125 000 to 135 000. Stage 3 covers all Reynolds numbers beyond Stage 2 and is limited only by the range covered in the experiments. The period of constant Reynolds

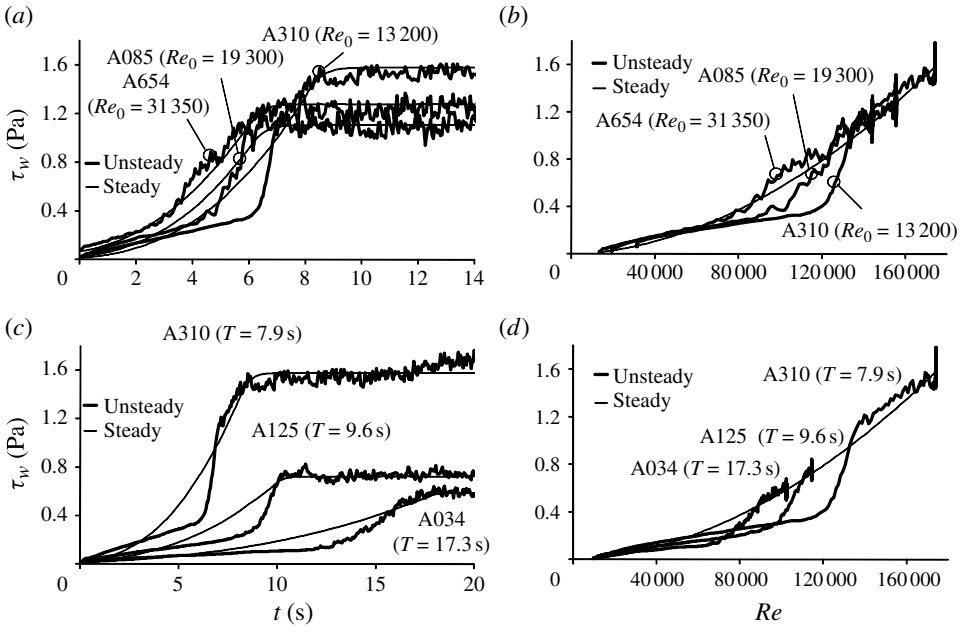

FIGURE 4. Variation of wall shear stress in ramp up flows. (*a*, *b*) influence of the initial Reynolds number; (*c*, *d*) influence of the acceleration.

number after the imposed acceleration ceases can be identified from the quasi-steady curves in figures 4(*a*) and 4(*c*). During Stage 1, the wall shear stress first exceeds the quasi-steady value and then falls below it. In some cases, this stage ends soon after the actual wall shear stress becomes smaller than the quasi-steady value. In others, however, it extends long after this instant and the actual stress is sometimes less than half the quasi-steady value. In Stage 2, the wall shear stress increases rapidly and monotonically (within experimental tolerances). Irrespective of the undershoot in the start of Stage 2, the wall shear stress at the end of the stage is slightly greater than the quasi-steady value. During Stage 3, the stress approaches the quasi-steady value asymptotically.

Figure 5 shows evolutions of the ensemble averaged r.m.s. of turbulent wall shear stresses (τ_w') for the two groups of experiments and the three stages are again seen. In contrast with the mean wall shear stress, which increases suddenly and then more slowly in Stage 1, τ_w' remains almost unchanged. This is followed by a period (Stage 2) when it increases rapidly, approaching the quasi-steady value in a short interval. Thereafter (Stage 3), it tends to be a little smaller than the quasi-steady value, but it evolves broadly in line with quasi-steady behaviour.

The variation of the turbulent wall shear stress shown above is characteristically similar to the three-stage response of turbulence previously measured in the core of the flow field (see for example He & Jackson 2000; Greenblatt & Moss 2004). Nevertheless, as discussed in § 3.3, some aspects of the behaviour of turbulence near the wall differ from the behaviour in the core region. At this stage, it is of most interest to note the broad similarity between the three-stage responses of the mean and turbulent shear stresses. This provides direct evidence that the response of the wall shear stress is associated with the turbulence response in the flow. That is, in Stage 1, the response of the shear stress at the wall reflects the condition that turbulence

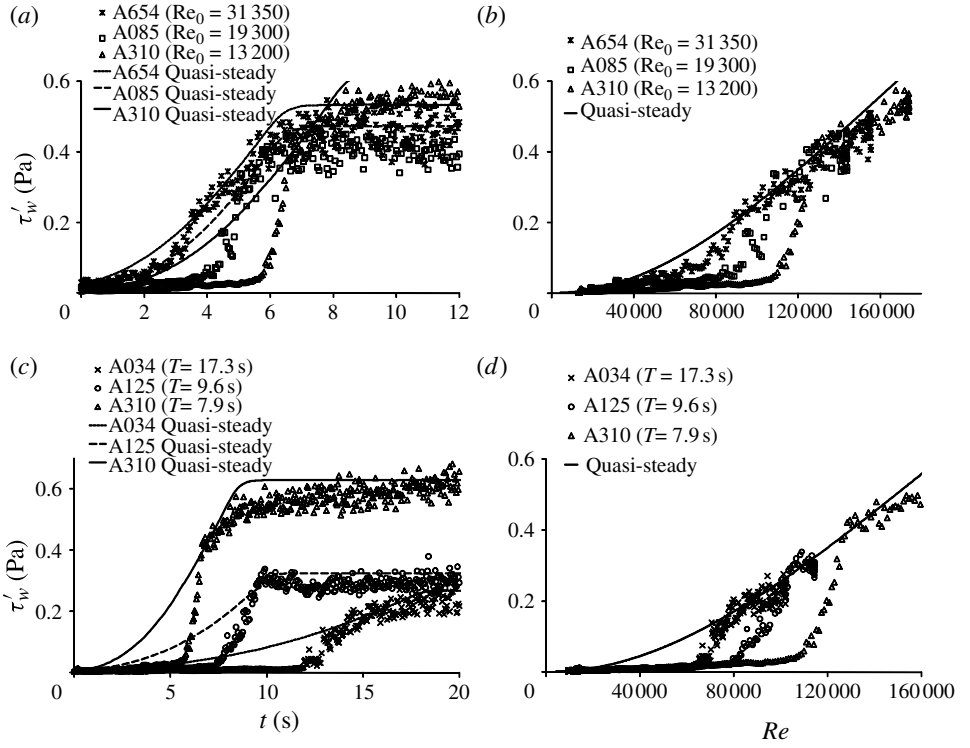

FIGURE 5. Variation of r.m.s. turbulent wall shear stress. (*a*, *b*): influence of the initial Reynolds number; (*c*, *d*): influence of the acceleration.

over the whole flow section remains largely frozen. As a result, and as discussed in detail below, the developing behaviour is driven mainly by flow acceleration (inertia). Next (Stage 2), the strong response of turbulence causes the mean wall shear to increase rapidly, approaching quasi-steady values as the turbulence evolves towards an equilibrium state (Stage 3). Consequently, the wall shear stress development can be conveniently described in terms of turbulence responses in the three stages, namely approximately frozen, transitional and quasi-equilibrium turbulence, respectively. For the same reasons, the first two stages can be regarded as delay and recovery stages.

The distinctive behaviours of the wall shear stress in the three stages are supportive of previous measurements by, for example, Ainola *et al.* (1983) and Proudovsky & Oreshkin (1985). At first sight, however, they are in conflict with the measurements reported by Shuy (1996), because all values of the ratio of the unsteady and quasi-steady wall shear stresses that he reported were smaller than unity. However, Shuy's measurements did not include the early stages of the accelerations, i.e. the data were for a period starting 5 s after the commencement of the acceleration. It is likely that his measurements corresponded to the later part of Stage 1 when the present experiments also yield values smaller than unity.

3.2. *Stage 1 responses*

It is now shown that the qualitative trends of the wall shear stress histories seen in figures 4 and 5 in Stage 1 can be expressed in a unified manner with the aid of simple theoretical considerations. The governing equation derived from the Reynolds averaged

Navier–Stokes equation for a spatially fully developed, axisymmetric unsteady pipe flow is

$$\frac{\partial \bar{u}}{\partial t} = -\frac{1}{\rho}\frac{\mathrm{d}\bar{p}}{\mathrm{d}x} + \frac{1}{r}\frac{\partial}{\partial r}\left[r\left(\nu\frac{\partial \bar{u}}{\partial r} - \overline{u''v''}\right)\right] \tag{3.1}$$

where $\bar{u}$ and $\bar{p}$ are the ensemble averaged mean velocity and pressure respectively, and $\overline{u''v''}$ is the ensemble averaged turbulent shear stress based on the axial and radial fluctuating velocities u'' and v''. The pressure gradient $\mathrm{d}\bar{p}/\mathrm{d}x$ is a function of time only (i.e. not of axial or radial position) and the initial *steady* flow just before the commencement of the flow excursion is described by

$$0 = -\frac{1}{\rho}\frac{\mathrm{d}\bar{p}_0}{\mathrm{d}x} + \frac{1}{r}\frac{\partial}{\partial r}\left[r\left(\nu\frac{\partial \bar{u}_0}{\partial r} - (\overline{u''v''})_0\right)\right], \tag{3.2}$$

where the suffix 0 denotes the steady flow condition during $t \leqslant 0$. Subtracting (3.2) from (3.1) gives

$$\frac{\partial \bar{u}^{\wedge}}{\partial t} = -\frac{1}{\rho}\frac{\mathrm{d}\bar{p}^{\wedge}}{\mathrm{d}x} + \frac{1}{r}\frac{\partial}{\partial r}\left[r\left(\nu\frac{\partial \bar{u}^{\wedge}}{\partial r} - (\overline{u''v''})^{\wedge}\right)\right] \tag{3.3}$$

where $\bar{u}^{\wedge} = \bar{u} - \bar{u}_0$, $\bar{p}^{\wedge} = \bar{p} - \bar{p}_0$, $(\overline{u''v''})^{\wedge} = (\overline{u''v''}) - (\overline{u''v''})_0$ and $-(1/\rho)(\mathrm{d}\bar{p}^{\wedge}/\mathrm{d}x) = -(1/\rho)(\mathrm{d}(\bar{p} - \bar{p}_0)/\mathrm{d}x) = -((1/\rho)(\mathrm{d}\bar{p}/\mathrm{d}x) - (1/\rho)(\mathrm{d}\bar{p}_0/\mathrm{d}x))$, denoting changes of the various quantities from their corresponding steady flow values.

Now we focus on Stage 1 where turbulence is nearly frozen. In the unsteady friction community, the 'frozen turbulence' is commonly interpreted as the eddy viscosity remaining unchanged (e.g. Vardy & Brown 2003). Under this assumption, $(\overline{u''v''})^{\wedge} = \nu_t(\partial\bar{u}/\partial y) - \nu_{t0}(\partial\bar{u}_0/\partial y)$ becomes $(\overline{u''v''})^{\wedge} = \nu_{t0}(\partial(\bar{u} - \bar{u}_0)/\partial y) = \nu_{t0}(\partial\bar{u}^{\wedge}/\partial y)$. By substituting this into (3.3), it is clear that the evolution of the flow field ($\bar{u}^{\wedge}$) will be affected by the initial turbulence through ν_{t0}.

Alternatively, 'frozen turbulence' can be interpreted as implying that the turbulent shear stress ($\overline{u''v''}$) remains unchanged from $(\overline{u''v''})_0$, namely,

$$(\overline{u''v''})^{\wedge} = (\overline{u''v''}) - (\overline{u''v''})_0 = 0. \tag{3.4}$$

There have not been sufficient measurements which can be used to discern which of the above assumptions is closer to reality although unpublished recent DNS results suggest that the former is closer to reality for a longer period than the latter. Nevertheless, the latter assumption (3.4) is adopted here because it leads to a much simpler formulation. Small deviations from reality are not a major concern for the purposes of this particular discussion because the analysis is used only to establish a framework for data reduction.

Using (3.4), (3.3) reduces to

$$\frac{\partial \bar{u}^{\wedge}}{\partial t} = -\frac{1}{\rho}\frac{\mathrm{d}\bar{p}^{\wedge}}{\mathrm{d}x} + \frac{\nu}{r}\frac{\partial}{\partial r}\left[r\frac{\partial \bar{u}^{\wedge}}{\partial r}\right] \tag{3.5}$$

where $\bar{u}^{\wedge} = 0$ at $t = 0$. The turbulent shear stress has now disappeared from the equation and so the *incremental velocity* ($\bar{u}^{\wedge} = \bar{u} - \bar{u}_0$) of the unsteady *turbulent* flow behaves approximately like an unsteady *laminar* flow accelerating from rest in response to an imposed time-varying pressure gradient $-(1/\rho)(\mathrm{d}\bar{p}^{\wedge}/\mathrm{d}x)$. The first two authors of this paper have taken this idea further and have shown from analytical solutions of (3.5) (now effectively a formulation for laminar flow) that the wall shear stress during Stage 1 in a *uniformly* accelerating turbulent flow (i.e. $\mathrm{d}U/\mathrm{d}t = const.$

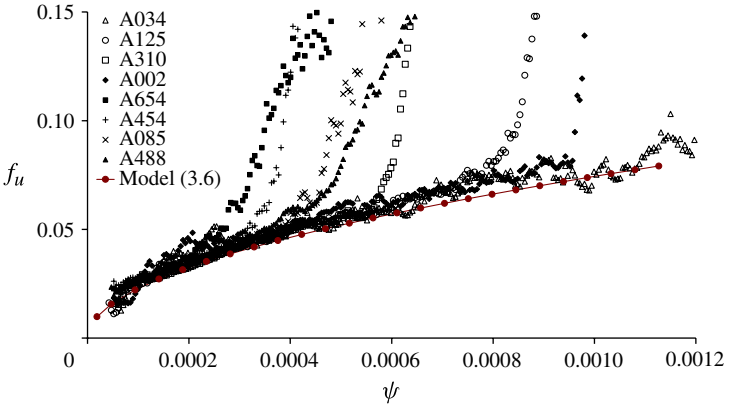

FIGURE 6. (Colour online) Dependence of normalized perturbation wall shear stress on normalized time.

where U is the bulk velocity) can be expressed as (He & Ariyaratne 2011):

$$f_u = \frac{4}{\sqrt{\pi}}\psi^{1/2} + 3\psi \tag{3.6}$$

where $f_u \equiv \tau_w^{\wedge}/((1/2)\rho R(\mathrm{d}U/\mathrm{d}t))$, $\tau_w^{\wedge} \equiv \tau_w(t) - \tau_w(0)$, $\psi \equiv \nu t/R^2$ and R is the radius of the pipe. That is, the normalized incremental wall shear stress is a function of the normalized time only.

In the present experiments, the acceleration $\mathrm{d}U/\mathrm{d}t$ is not exactly constant, but varies with time. To utilize the general idea of (3.6), $\mathrm{d}U/\mathrm{d}t$ is replaced by the instantaneous acceleration. This enables the experimental data to be presented in the non-dimensional form shown in figure 6, from which it is apparent that, in Stage 1, data for all experiments collapse almost onto a common curve that is independent of the acceleration and of the initial Reynolds number. The curve is consistently above the prediction based on (3.6), but not greatly so, thereby suggesting that the unsteady component of the flow does indeed behave almost in a laminar-like manner. In other words, the *differential* wall shear stress $(\tau_w(t) - \tau_w(0))$ depends primarily on the flow acceleration (inertia). As far as this quantity is concerned, not only is the turbulence almost frozen, but also the level of initial turbulence or indeed its existence is irrelevant. The differences between predictions of (3.6) and the experimental data cannot be attributed to experimental uncertainties. Instead, they arise because (i) the flow acceleration is not linear and (ii) turbulence does not remain completely unchanged. The latter is discussed below.

Although the increase of turbulent wall shear stress is small in comparison with the increase of quasi-steady values (figure 5), the increasing trend is clearly identifiable. To investigate this trend, figure 7 shows the turbulence intensity for a range of cases studied, i.e. τ_w' normalized using the corresponding mean wall shear stress. The relatively large scatters are the results of small ensemble samples (of the order of 100). Nevertheless, the trends are persistent. Immediately after the commencement of the flow exertion, the intensity reduces rapidly to a low level and then remains nearly constant throughout the delay period. This constant level of wall turbulence intensity is of significant interest, implying that the rate of increase of τ_w' is directly proportional to that of the mean wall shear itself throughout most of Stage 1 although at a much lower level than in a steady flow. In some cases, this means that the

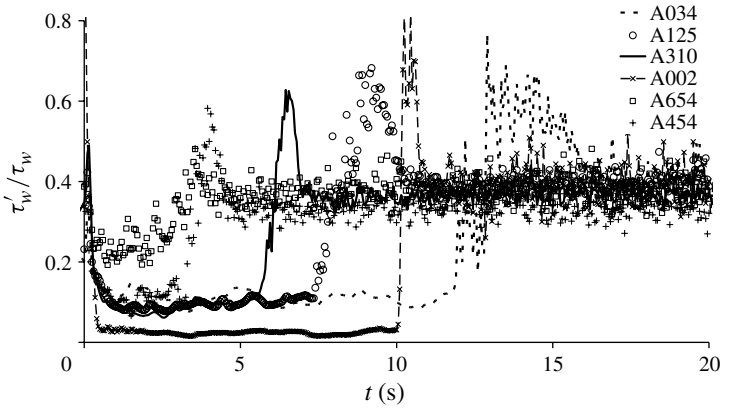

FIGURE 7. Evolution of turbulent wall shear stress normalized using mean wall shear stress (turbulence intensity) in a number of unsteady flows.

absolute value of the turbulent shear stress increases by several times towards the end of Stage 1 in spite of it being much lower than in a steady flow. At first sight, this observation appears to contradict the concept of 'frozen' turbulence in the early stage of response discussed above. However, the following hypothesis is offered to reconcile the apparent conflict. Following the conclusions of previous studies, assume that no *new* turbulence structures (bursts) are produced in Stage 1, during which the influence of the flow acceleration on the velocity gradient is confined primarily to a region very close to the wall ($y^+ < 5$, say). Turbulent activities/eddies at this stage are those associated with the initial conditions before the commencement of the acceleration. Along with the increase of the velocity gradient, these eddies are stretched streamwise near the wall, leading to increased fluctuations in the stream velocity and hence to the observed increases in τ_w'. This increase is proportional to the increase of the bulk velocity (hence, the constant intensity in figure 7), but it is nevertheless much smaller than would exist in a quasi-steady flow. During this period, there is little direct influence on the other two velocity components. Although no direct measurements of turbulence close to the wall are available to assess this hypothesis, measurements in the buffer and core regions in previous studies (He & Jackson 2000; Greenblatt & Moss 2004) are consistent with it. That is, they show slow, but definite, increases in streamwise turbulent fluctuations, but not in normal and spanwise fluctuations. More directly, a DNS study of a *spatially* accelerating flow by Piomelli *et al.* (2000) has shown that turbulent structures are significantly stretched in the stream direction as a result of flow acceleration.

The steady value of the turbulence intensity of the wall shear stress (τ_w'/τ_w) in Stage 1 (figure 7), referred to herein as the *Stage 1 turbulent wall shear intensity*, ranges from 0.02 in case A002 to 0.2 in case A654, showing that it is influenced by both the initial Reynolds number and the acceleration. A closer inspection reveals that, as a trend, the Stage 1 turbulent intensity increases with the increase of the initial Reynolds number, but reduces with the increase of the flow acceleration. To quantify the effects, non-dimensional parameter groups have been sought to correlate Stage 1 turbulent intensity. In particular, the acceleration parameter group $((1/U_0)(\mathrm{d}U/\mathrm{d}t))$ was combined with an 'inner', 'outer' and a 'mixed' time scale, $\nu/U_{\tau 0}^2$, D/U_0 and $D/U_{\tau 0}$ leading to $(\nu/U_{\tau 0}^2)((1/U_0)(\mathrm{d}U/\mathrm{d}t))$, $(D/U_0)((1/U_0)(\mathrm{d}U/\mathrm{d}t))$ and $(D/U_{\tau 0})((1/U_0)(\mathrm{d}U/\mathrm{d}t))$. These are all based on initial

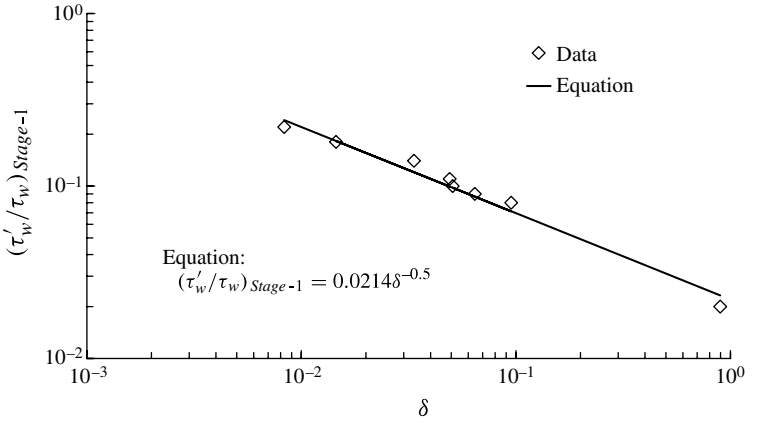

FIGURE 8. Correlation of maximum reduction of turbulent wall shear stress intensity.

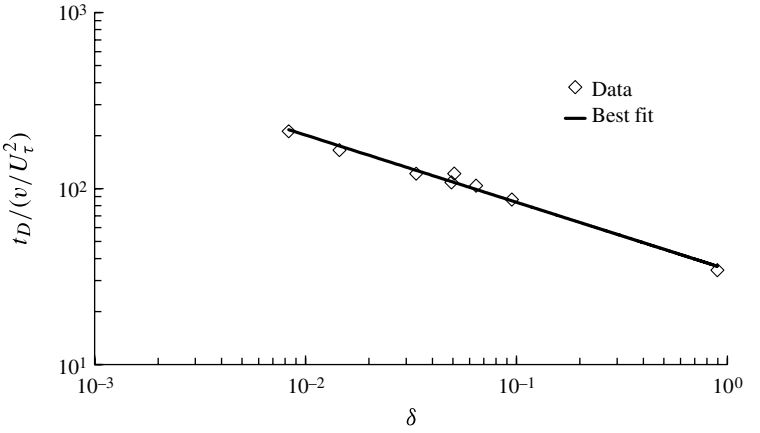

FIGURE 9. Correlation of the delay of wall turbulence.

flow conditions. Figure 8 shows that the Stage 1 turbulent wall shear intensity is well correlated using the inner-scale based parameter, but the other two parameters failed to correlate the data (results are not shown). As shown in the figure, the data is well represented by the expression

$$\left(\frac{\tau_w'}{\tau_w}\right)_{Stage\text{-}1} = 0.0214\delta^{-0.5} \tag{3.7}$$

where $\delta = (\nu/U_{\tau 0}^2)(1/U_0)(\mathrm{d}U/\mathrm{d}t)$. This equation shows that, for a given fluid, Stage 1 turbulent intensity is approximately proportional to the initial friction velocity and inversely proportional to the square root of the (relative) flow acceleration $((1/U_0)(\mathrm{d}U/\mathrm{d}t))$. It is worth noting that the largest starting Reynolds number covered in this study is ~31 000 which is still quite low and the validity of the results for high Reynolds number flows needs to be checked. Similar caution needs to be applied to results presented in figures 9 and 10.

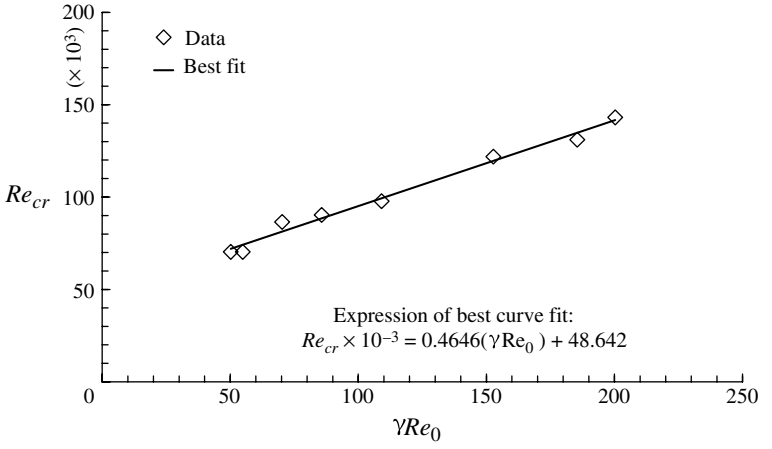

FIGURE 10. Critical Reynolds number at the transition from Stage 1 to Stage 2.

3.3. *Stages 2 and 3 responses*

Figure 5 shows that the response of the turbulent wall shear stress is influenced by the initial Reynolds number and also by the acceleration. For any particular acceleration, the duration of Stage 1 reduces with increasing initial Reynolds number and the critical Reynolds number at which turbulence response begins also reduces. In contrast, for any particular initial Reynolds number, the duration of Stage 1 reduces with increasing acceleration, but the critical Reynolds number increases.

This behaviour can be compared with the response of turbulence in the *core* of the flow, as measured by He & Jackson (2000). They found that, for a given acceleration, the duration of Stage 1 in the core decreases with increasing initial Reynolds number as it does at the wall. However, in contrast with the present wall measurements, they found that, for a given initial Reynolds number, the absolute delay time of the turbulence response in the core of the flow (i.e. the duration of Stage 1) is independent of the acceleration rate. At the centre of the pipe, for example, this delay was found to scale with $D/U_{\tau 0}$, hence being a function of the initial Reynolds number, but not of the acceleration. Thus, the consequences of the flow response mechanisms in the core and at the wall are different.

As mentioned earlier, it has been established in previous studies that in an accelerating flow, turbulence first responds in the buffer layer and this response then propagates into the core as well as towards the wall. Hence, in both the core and the wall regions, delays arise from two causes, namely (i) delays before significant production of new turbulence begins in the buffer layer and (ii) the time needed for the consequences of the new turbulence to be detected at the measuring location. The first of these is common to all measurement locations, but the second is not. In the core region, the second phenomenon is typically much greater than the first and the time needed for new turbulence to diffuse inwards dominates the overall delay. In contrast, the time needed for the turbulence to propagate outwards through the viscous layer to the wall is quite small and so the two components are of a similar order. Based on this interpretation, the measured influence of acceleration on delay times at the wall can arise in two ways. The more obvious of these is that larger accelerations reduce the time before new turbulence begins. This is consistent with measurements in the buffer layer by He & Jackson (2000) and also, for pulsating channel flows, by Tardu

& Binder (1993). In addition, the Reynolds number at which new turbulence begins is higher for a higher acceleration, and this increased Reynolds number in turn leads to a thinner viscous sublayer. This then reduces the time needed for the fluctuations to diffuse across it.

Figure 9 shows that the delay time at the wall (i.e. the duration of Stage 1) can be correlated using the inner scale based parameter δ used in figure 8, which evidently takes effective account of the two influencing factors, namely, the initial Reynolds number and the acceleration. The normalized delay is seen to reduce strongly with increasing values of δ and the dependence can be represented quite well by a power law function, noting the use of the double logarithmic scale in the figure.

The critical Reynolds number at which significant new turbulence is detected at the wall can be identified from figure 7 as the point when the turbulent intensity starts to increase rapidly. Figure 10 shows that the critical Reynolds number determined this way for the various test cases can be correlated quite well with a parameter group γRe_0, where $\gamma = (D/U_{\tau 0})((1/U_0)(\mathrm{d}U/\mathrm{d}t))$. The data are closely represented by a linear relationship:

$$Re_{cr} \times 10^{-3} = 0.4646(\gamma Re_0) + 48.642. \tag{3.8}$$

The parameter group γRe_0 can be rearranged as $(1/Re_{U_{\tau 0}})((\mathrm{d}U/\mathrm{d}t)(D^3/\nu^2))$, where the friction Reynolds number (or Kármán number) $Re_{U_{\tau 0}} = U_{\tau 0}D/\nu$. That is, the critical Reynolds number is directly proportional to the normalized acceleration $(\mathrm{d}U/\mathrm{d}t)(D^3/\nu^2)$, but inversely proportional to the starting Reynolds number $Re_{U_{\tau 0}}$. The dependence on acceleration is analogous to the delayed transition from laminar to turbulent flow in the presence of acceleration. Recently Knisely, Nishihara & Iguchi (2010) proposed a simple empirical expression that correlates well all of the data that they have found from the literature as well as their own data on transitional Reynolds number in accelerating flows starting from a laminar flow or from rest. The expression reads

$$Re_{tr} = 1.33\left(\frac{\mathrm{d}U}{\mathrm{d}t}\frac{D^3}{\nu^2}\right)^{1.83/3}. \tag{3.9}$$

It is interesting that the same parameter group, $(\mathrm{d}U/\mathrm{d}t)(D^3/\nu^2)$, appears in both (3.8) and (3.9), but the former also includes a term that is dependent on the starting Reynolds number whereas the latter does not.

In the discussion so far, little attention has been paid to phase differences between the responses of the mean and turbulent wall shear stresses such as those illustrated in figure 11 for a typical case (A125). These phase differences have a strong influence on the turbulence intensity (τ_w'/τ_w) shown in figure 7. Under steady conditions, the flow is in an equilibrium state and a direct correlation exists between the turbulent and mean shear stresses, the intensity being $\sim$0.4 irrespective of Reynolds number (note that Tardu & Binder 1993 deduced 0.3–0.4 for a channel flow). The intensity tends to reduce strongly in Stage 1, then increases sharply at the beginning of Stage 2, before settling back to a sustained level more characteristic of quasi-steady flow at the start of Stage 3. That is, a strong increase in τ_w' occurs *before* the rapid response in the mean wall shear stress. During this period, the turbulence is strongly non-equilibrium and near the wall it can be strongly out of phase with turbulence elsewhere in the cross section. It is noted that when the value of τ_w'/τ_w is very large, there may be instantaneous flow reversals and, under such a condition, hot-film measurements embed higher uncertainties. However, this affects only a very limited number of measurements in the present study.

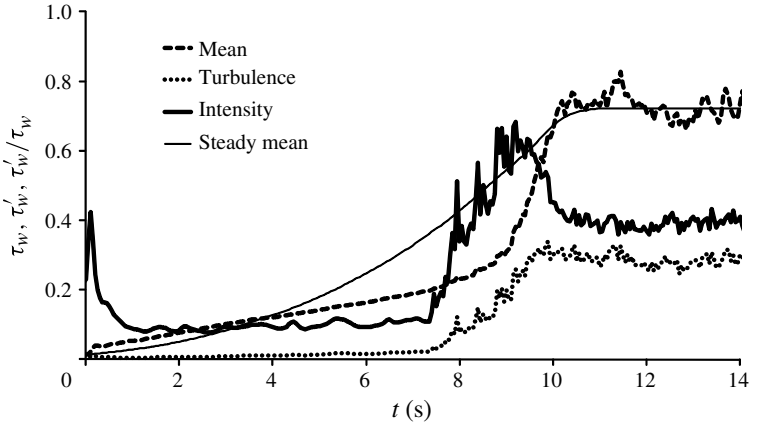

FIGURE 11. Comparison of responses of mean and turbulent wall shear stresses (A125).

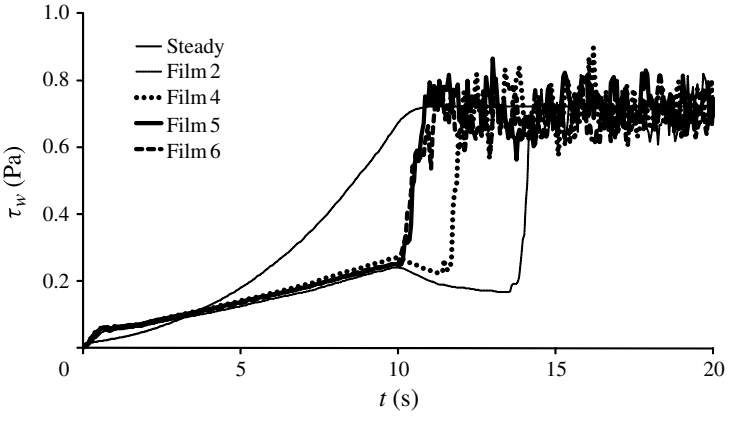

FIGURE 12. Wall shear stress in a 'short' transient flow and its non-uniform circumferential distribution (A002).

Before closing the paper, attention is drawn to particular flows in which the period of mean acceleration ended whilst the flow was still in Stage 1. Figure 12 shows wall shear stresses measured by four hot-film sensors in case A002. Three films (i.e. 4, 5 and 6) were at one axial location and the fourth (film 2) was at the other (see figure 1). Film 6 was at the bottom of the pipe and films 2, 4 and 5 were at 120° points in the upper half of the pipe.

One clear conclusion from figure 12 is that the flow behaved in a non-axisymmetric manner. The measurements of films 5 and 6 are similar to each other, but they differ strikingly from those of film 4 at the same axial location. The transition (Stage 2) at film 4 occurs almost 2 s later than that at films 5 and 6. For a brief period at around 11 s, the ratio of the stresses measured by films 4 and 6 differs by a factor of about 3. This contrasts with the behaviour in cases in which the transition occurred whilst the favourable pressure gradient was still present and the flow was accelerating. In these flows, the three-dimensionality was much weaker, as illustrated in figure 3, for example. That is, the stabilizing effect of the flow acceleration not only caused the critical Reynolds number to increase, but also reduced asymmetry.

Strong asymmetry was also measured experimentally by Brunone *et al.* (2000) and predicted theoretically by Ghidaoui & Kolyshkin (2001) for oscillatory water hammer flows. It was demonstrated in both studies that asymmetry is phase-dependent and is more likely to occur in a decelerating flow than in an accelerating one. Das & Arakeri (1998) and Zhao, Ghidaoui & Kolyshkin (2007) also studied the laminar–turbulent transition in unsteady flows and concluded that it is likely to be caused by asymmetric instability.

Figure 12 also shows the response of the wall shear stress when the acceleration ceases during Stage 1. During the acceleration, the stress increases continuously and this has been reconciled above with a gradually evolving velocity profile in an effectively frozen-stress environment. After the acceleration ceases, however, there is a marked change of behaviour. Films 5 and 6 show sharp increases characteristic of the onset of Stage 2, whereas films 2 and 4 experienced a period of gradually reducing stress before Stage 2 commenced. The reduction is consistent with a gradual relaxation of the velocity profile from the form that exists during the steady acceleration to the form that would exist in a steady flow with the same turbulent viscosity distribution. The asymmetry of the responses (i.e. films 2 and 4 versus films 5 and 6) complicates the picture, but it seems reasonable to infer that the frozen-turbulence state is not inherently sensitive to changes in the acceleration, even though the mean wall shear does respond to it.

4. Conclusions

An experimental study of accelerating flow in a pipe has been reported, in which wall-mounted hot-film sensors have been used to obtain ensemble-averaged mean and r.m.s. values of turbulent wall shear stresses. The *mean wall shear stress* has been shown to respond to an imposed acceleration in three stages. Stage 1 begins immediately after the onset of the acceleration. In this stage, the wall shear stress initially increases rapidly, overshooting the quasi-steady value, and then increases more gradually, at a much slower rate than would apply if the flow behaved in a quasi-steady manner. The turbulence state is nearly frozen and the incremental wall shear $(\tau_w(t) - \tau_w(0))$ depends primarily on the acceleration, not on the initial flow conditions including the initial turbulence. In this stage, the incremental wall shear stress can be predicted quite well by a laminar flow formulation. In Stage 2, the wall shear stress increases rapidly to a value that is close to the quasi-steady equivalent. Significant phase differences exist between the response of the turbulent wall shear and the mean wall shear. These have been explained in relation to the time needed for fluctuations to propagate into the core of the pipe. In Stage 3, both the turbulent wall shear and the mean wall shear are close to values expected in a flow behaving in a quasi-steady manner. In general, the characteristic behaviour of the conditions at the wall has been related to the combined influences of inertia and turbulence response.

In Stage 1, the *turbulent wall shear stress* does not remain completely frozen but increases steadily although at a smaller rate than in a quasi-steady flow. In Stage 2, it increases rapidly, overshooting the quasi-steady value and then relaxing towards it. In Stage 3, it fluctuates around the quasi-steady value. The steady increase in Stage 1 is attributed to the stretching of the turbulence eddies existing at the beginning of the flow acceleration, such stretching being associated with increasing mean velocity gradient near the wall. The subsequent rapid increase of τ_w' in Stage 2 is attributed to the generation of new turbulence.

The turbulent wall shear stress *intensity* reduces strongly at the beginning of Stage 1, but then remains constant throughout this stage, indicating that the ratio of the rate of increase of turbulent stress and that of the mean shear stress remains constant. This intensity reduces with increasing acceleration and with decreasing initial Reynolds number.

The delays in the responses of the mean and turbulent wall shear stresses increase with increasing acceleration and decrease with increasing initial Reynolds number. The latter contrasts with the response of turbulence in the core of the flow, where the delays are independent of the rate of acceleration. The response at the wall is strongly influenced by turbulence production time scales whereas the response in the core is dominated by the larger time scales associated with radial propagation. The measured delays in the various tests and also the Reynolds numbers at transition to Stage 2 have been shown to correlate in a simple manner with a non-dimensional parameter δ characterizing the initial flow state and the subsequent mean acceleration.

The authors gratefully acknowledge that the work reported in this paper was sponsored through EC-HYDRALAB III Contract 022441 (R113) and the UK Engineering and Physical Sciences Research Council (EPSRC) through grants EP/C015177/1 and EP/C015479/1.

REFERENCES

AINOLA, L., KOPPEL, T., LAMP, J. & LIIV, U. 1983 The skin friction coefficient during accelerated flows in pipes. In *Proceedings XX IAHR Congress, Moscow, USSR*, vol. 6, pp. 453–460.

ARIYARATNE, C., WANG, F., HE, S. & VARDY, A. E. 2010. Use of hot-film anemometry for wall shear stress measurements in unsteady flows. In *International Heat Transfer Conference. August 8–13, Washington DC, USA, IHTC14-22674*.

BRERETON, G. J. & REYNOLDS, W. C. 1991 Dynamic response of boundary-layer turbulence to oscillatory shear. *Phys. Fluids* A **3**, 178–187.

BRERETON, G. J., REYNOLDS, W. C. & JAYARAMAN, R. 1990 Response of a turbulent boundary layer to sinusoidal free stream unsteadiness. *J. Fluid Mech.* **221**, 131–159.

BRUNONE, B., KARNEY, B. W., MICARELLI, M. & FERRANTE, M. 2000 Velocity profiles and unsteady pipe friction in transient flow. *J. Water Resour. Plng Mgmt ASCE* **126** (4), 236–244.

CHEW, Y. T., KHOO, B. C., LIM, C. P. & TEO, C. J. 1998 Dynamic response of a hot-wire anemometre. Part II: A flush-mounted hot-wire and hot-film probes for wall shear stress measurements. *Meas. Sci. Technol.* **9**, 764–778.

CHUNG, Y. M. 2005 Unsteady turbulent flow with sudden pressure gradient changes. *Intl J. Numer. Meth. Fluids* **47**, 925–930.

DAS, D. & ARAKERI, J. H. 1998 Transition of unsteady velocity profiles with reverse flow. *J. Fluid Mech.* **374**, 251–283.

GERRARD, J. H. 1971 An experimental investigation of pulsating turbulent water flow in a tube. *J. Fluid Mech.* **46**, 43–64.

GHIDAOUI, M. S. & KOLYSHKIN, A. A. 2001 Stability analysis of velocity profiles in water–hammer flows. *J. Hydraul. Engng ASCE* **127** (6), 499–512.

GREENBLATT, D. & MOSS, E. A. 1999 Pipe-flow relaminarization by temporal acceleration. *Phys. Fluids* **11**, 3478–3481.

GREENBLATT, D. & MOSS, E. A. 2004 Rapid temporal acceleration of a turbulent pipe flow. *J. Fluid Mech.* **514**, 65–75.

HE, S. & ARIYARATNE, C. 2011 Wall shear stress in the early stage of unsteady turbulent pipe flow. *J. Hydraul. Engng* **137**, 606–610.

HE, S., ARIYARATNE, C. & VARDY, A. E. 2008 A computational study of wall friction and turbulence dynamics in accelerating pipe flows. *Comput. Fluids* **37**, 674–689.

HE, S. & JACKSON, J. D. 2000 A study of turbulence under conditions of transient flow in a pipe. *J. Fluid Mech.* **408**, 1–38.

HE, S. & JACKSON, J. D. 2001 Wall shear stress in accelerating pipe flows. In *Energy Conversion and Application (Proceedings International Conference on Energy Conversion & Application, Wuhan, China)*. pp. 442–448.

HE, S. & JACKSON, J. D. 2009 An experimental study of pulsating turbulent flow in a pipe. *Eur. J. Mech. (*B/*Fluids*) **28**, 309–320.

KASAR, S., SHAH, R. K. & AUNG, W. 1987 *Handbook of Single-Phase Convective Heat Transfer*. John Wiley & Sons.

KNISELY, C. W., NISHIHARA, K & IGUCHI, M. 2010 Critical Reynolds number in constant-acceleration pipe flow from an initial steady laminar state. *J. Fluids Engng* **123**, 091202.

MAO, Z. & HANRATTY, T. J. 1986 Studies of wall shear stress in a turbulent pulsating pipe flow. *J. Fluid Mech.* **170**, 545–564.

MAO, Z. & HANRATTY, T. J. 1992 Measurement of wall shear rate in large amplitude unsteady reversing flows. *Exp. Fluids* **12**, 342.

MARUYAMA, T., KURIBAYASHI, T. & MIZUSHIMA, T. 1976 The structure of turbulence in transient pipe flows. *J. Chem. Engng Japan* **9**, 431–439.

PIOMELLI, U., BALARAS, E. & PASCARELLI, A. 2000 Turbulent structures in accelerating boundary layers. *J. Turbul.* **1**, 1–16.

PROUDOVSKY, A. M. 1997 Wall shear stress in accelerating and decelerating pipe flows. *J. Hydraul. Res.* **35** (1), 133–136.

PROUDOVSKY, A. M. & ORESHKIN, O. F. 1985 The characteristics of unsteady fluid flows. In *Proceedings of XXI IAHR Congress Seminar 3, Melbourne*.

RAMAPRIAN, B. R. & TU, S. W. 1983 Fully developed periodic turbulent pipe flow. Part 2. The detailed structure of the flow. *J. Fluid Mech.* **137**, 59–81.

RONNEBERGER, D. & AHERENS, C. D. 1977 Wall shear stress caused by small amplitude perturbations of turbulent boundary-layer flows: an experimental investigation. *J. Fluid Mech.* **83**, 433–464.

RUEDI, J. D., NAGIB, H., OSTERLUND, J. & MONKEWITZ, P. A. 2004 Unsteady wall-shear measurements in turbulent boundary layers using MEMS. *Exp. Fluids* **36**, 393–398.

SCOTTI, A. & PIOMELLI, U. 2001 Numerical simulation of pulsating turbulent channel flow. *Phys. Fluids* **13**, 1367–1384.

SHEMER, L., WYGNANSKI, I. & KIT, E. 1985 Pulsating flow in a pipe. *J. Fluid Mech.* **153**, 313–337.

SHUY, E. B. 1996 Wall shear stress in accelerating and decelerating turbulent pipe flows. *J. Hydraul. Res.* **34**, 173–183.

TARDU, S. F. & BINDER, G. 1993 Wall shear stress modulation in unsteady turbulent channel flow with high imposed frequencies. *Phys. Fluids A* **5**, 2028–2037.

TARDU, S. F., BINDER, G. & BLACKWELDER, R. F. 1994 Turbulent channel flow with large-amplitude velocity oscillations. *J. Fluid Mech.* **267**, 109–151.

TARDU, S. F. & DA COSTA, P. 2005 Experiments and modelling of an unsteady turbulent channel flow. *AIAA J.* **43**, 140–148.

TARDU, S. F. & PHAM, C. T. 2005 Response of wall hot-film gages with longitudinal diffusion and heat conduction to the substrate. *Trans. ASME: J. Heat Transfer* **127**, 812–819.

TU, S. W. & RAMAPRIAN, B. R. 1983 Fully developed periodic turbulent pipe flow. Part 1. Main experimental results and comparison with predictions. *J. Fluid Mech.* **137**, 31–58.

VARDY, A. E. & BROWN, J. M. B. 2003 Transient turbulent friction in smooth pipe flows. *J. Sound Vib.* **259**, 1011–1036.

ZHAO, M., GHIDAOUI, M. S. & KOLYSHKIN, A. A. 2007 Perturbation dynamics in unsteady pipe flows. *J. Fluid Mech.* **570**, 129–154.